International Journal Of Engineering Research And Development
e- ISSN: 2278-067X, p-ISSN: 2278-800X, www.ijerd.com
Volume 20, Issue 12 (December, 2024), PP 53-67

Geomechanical Analysis and Mud Weight Optimization for Wellbore Stability in Masa Field Niger Delta

Ohuobah, Larry Chiebuka[1], Professor Joel Ogbonna[2] and Okujagu, Diepiriye C[3]
[1]*Centre for Petroleum Geosciences, University of Port Harcourt*
[2]*Department of Petroleum Engineering, University of Port Harcourt*
[3]*Department of Geology, Faculty of Science, University of Port Harcourt*
diepiriye.okujagu@uniport.edu.ng (Corresponding author)

ABSTRACT
One of the challenges facing a well's life cycle is wellbore instability. Issues such as collapse of borehole, lost of circulation, stucking of pipe and production of sand results in non-productive time (NPT) which is a major off-shoot of wellbore instability. Well log suits [gamma ray, resistivity, sonic, density, neutron and V_{sh} logs] were used to deduce the rock mechanical characteristics for wellbore stability management. The depth of investigation ranges from 6000m-11000m of the stratigraphic unit of normal to abnormal pressured sandstone and shales. The volume of shale across the field ranges from 0.05 – 1.00m^3, vertical stress magnitude from 11.09 – 94.99 MPa/km, maximum effective horizontal stress from 42 – 87.02 MPa/km, & minimum effective horizontal stress from 12.20 – 52.70 MPa/km depicting a normal stress regime according to Aderson (1951) $\sigma v \geq \sigma_H \geq \sigma_h$. The formation pressure increases with depth throughout the field ranges from 19.2364 – 35.2667 MPa/m; fracture pressure gradient from empirical correlations are: 2.7958 x 10^{-3} MPa/m for Eaton's correlation; 3.1626 x 10^{-3}MPa/m for Mathew's and Kelly; ; 4.4354 x 10^{-3} MPa/m for Hubbert and Willis (min.) and 6.6534 x 10^{-3} MPa/m for Hubbert and Willis (max) and the window for the weight of the mud varies between 7.7 – 18.20 ppg with depth across the field which can be attributed to heterogeneity and anisotropy. These data can be useful during well drilling design program, optimization of production and other wellbore stability tasks.

Keywords: *Wellbore Stability, Geomechanical Properties, Formation Pressure Gradients, Well Log Analysis, Non-Productive Time (NPT), Stress Regime, Mud Weight Optimization*

Date of Submission: 01-12-2024 Date of Acceptance: 10-12-2024

I. INTRODUCTION

Wellbore instability represents one of the most significant challenges in petroleum drilling operations, accounting for approximately 10% of total drilling costs and resulting in annual industry losses ranging from $100 million to $1 billion globally. During drilling operations, wellbore instability can manifest through various mechanisms, including brittle deformation, plastic rock flow, and tensile rock splitting, each presenting unique challenges to drilling engineers and operators. The stability of a wellbore is fundamentally influenced by the complex interplay of geological factors, tectonic conditions, and material properties of the formation. A comprehensive understanding of these factors is essential for successful drilling operations, particularly given that approximately 90% of instability incidents occur in shale formations. The consequences of wellbore instability are far-reaching, leading to substantial operational challenges such as tool loss, expensive casing trips, side-tracking requirements, excessive reaming time, and compromised logging and cementing conditions. Geomechanical modeling has emerged as a critical tool in addressing these challenges. A complete geomechanical model incorporates six key components: vertical stress (σv), maximum horizontal stress (σHmax), minimum horizontal stress (σhmin), stress direction (σHmax Azi), pore pressure (PP), and rock strength (UCS). These parameters provide the foundation for understanding and predicting wellbore behavior during drilling operations.

This study focuses on developing an optimized mud weight window for specific stratigraphic depths through the analysis of geomechanical properties derived from well logs and empirical calculations. By utilizing a linear-elastic geomechanical model incorporating Eaton's correlation, Matrix Stress analysis, Young's Modulus, Poisson's ratios, and established frameworks from Hubbert and Willis and Mathew and Kelly, this research aims to enhance drilling efficiency and reduce non-productive time (NPT). The findings of this study have significant implications for both wellbore stability management and hydraulic fracture treatment strategies.

II. Literature Review

When we talk about the stabilization of the wellbore, we are talking to the wellbore's capacity to guarantee that its gauge or near-gauge value does not vary over time (Jiang et al., 2022). The competency in issue is the one that we are referring to in this particular setting. A relationship exists between the resistance of the formation and the interaction that takes place between the stresses that are present in the formation and their transposed forms. This interaction gives rise to the formation's resistance (Radwan, 2022). There exists a correlation between the strength of the formation and this contact. (Kamgue et al., 2023). The formation is so potent because of the interaction between these two components, which is what makes it so effective (Teodoriu & Bello, 2021). As demonstrated in Figure 1, one of the most common manifestations of wellbore instability is tight hole or stuck pipe conditions. The instability that resulted from this interaction was a consequence of the stress imbalance. As a result of the fact that it is responsible for extra expenditures that amount to more than one billion dollars (10–15 percent of the entire cost of the well) each year all over the globe, wellbore instability continues to be a challenging and expensive obstacle for drilling operations (Wood, 2024).

In the majority of situations, the rock is in a stable state prior to the drilling of a borehole; nonetheless, the stability of the rock is lowered as a consequence of the excavation process. Figure 2 illustrates various indications of wellbore instability, while Figure 3 presents the primary causes that lead to these stability issues. The use of drilling mud is possible to make a contribution to the prevention of rock collapse. This is because drilling mud helps to keep the field in a state of balance while the drilling operation is being carried out. There are a number of wellbore stability signals, some of which include, but are not limited to, the following: breakout, collapse, under-gauged hole, cavings at surface, excessive volume of cuts and cavings, elevated circulation pressures, unexpected side-tracks, and even abandonment. As shown in Figure 4, these symptoms of excessive stresses can manifest in various ways. Additionally, Figure 5 specifically illustrates how shale swelling can result in instability, which is a common problem in many formations. In situations when the stress rock strength is lower than the stress in the wellbore, it is reasonable to assume that rock mechanical failure will take place at some point in time. This is particularly relevant in the Niger-Delta Basin, whose generalized geologic map is shown in Figure 6. The region's complex geology, including its characteristic depo-belts (Figure 7, Modified after Onikoyi et. al., 2014), contributes significantly to wellbore stability challenges.

The schematic dip section of the Niger-Delta (Figure 8, Modified from Doust and Omatsola, 1990 and Stakicher, 1995) reveals the complex stratigraphic relationships that must be considered during drilling operations. Typical growth faults, as illustrated in Figure 9, along with various oil field structures and associated trap types (Figure 10, Modified from Doust and Omatsola, 1990 and Staicher, 1995), further complicate drilling operations in the region. The presence of shale tectonics, shown in Figure 11, adds another layer of complexity to wellbore stability considerations.

The collection of data on geo-mechanical parameters, which may be collected via drilling cores or wireline logs, is an absolutely necessary step in the process of constructing and maintaining a wellbore that is stable. There are a variety of different approaches that can be taken to acquire this information. Using wireline logs, which guarantees that logs are continually present throughout the whole of the reservoir rocks, is one of the aspects that contributes to the successful results that are produced. On the other hand, core samples are never made available for review prior to the beginning of the drilling technique, despite the fact that they provide superior results. Specifically, this is because core samples are considered to be of more value than other types of samples (Azizi and Memarian, 2015).

Figure 1: Tight Hole or Stuck pipe
Source: Drilling Formulas.com (2024): Powered by Mandra & World press

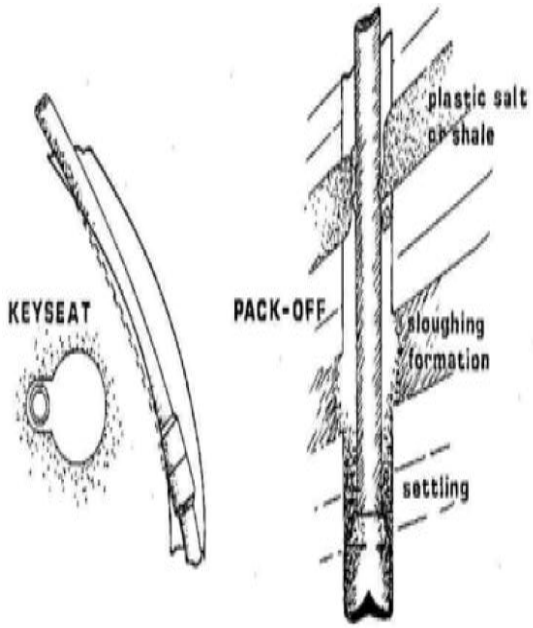

Figure 2: Indications of wellbore instability
Source: Agushoe. (2011).

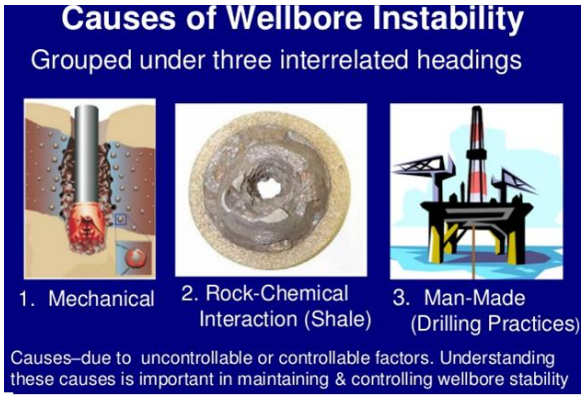

Figure 3: causes of wellbore instability
Source: Bowling, (2012).

Figure 4: symptoms of excessive stresses
Source: Bowling, (2012).

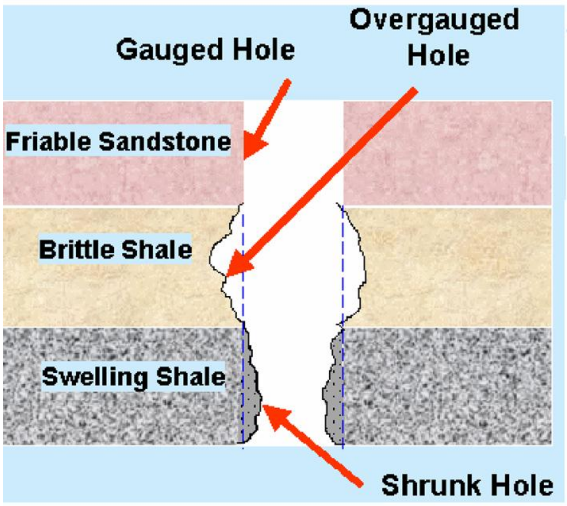

Figure 5: shale swelling resulting in instability
Source: Bowling, (2012).

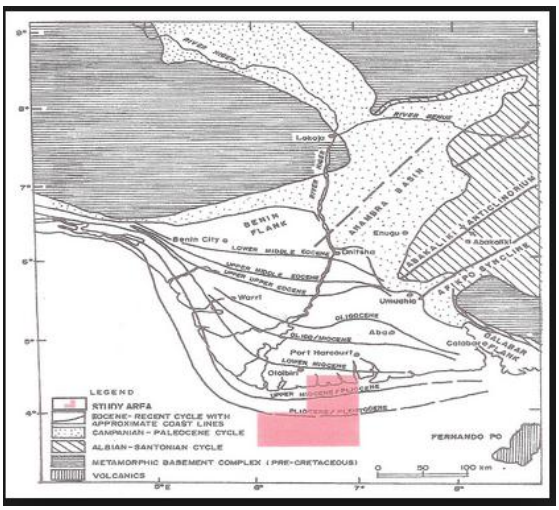

Figure 6: Generalized Geologic map of Niger-Delta Basin
Source: Short and Staubple (1967): United States Geological Survey)

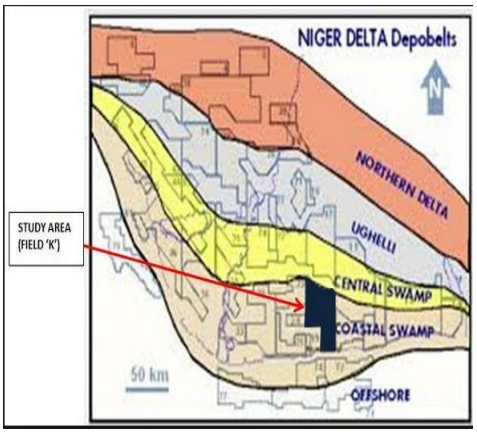

Figure 7: Niger-Delta Depo-belts. (Modified after Onikoyi et. al., 2014)

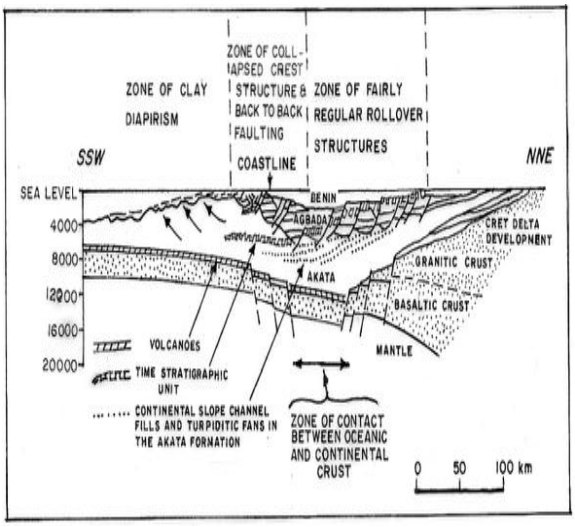

Figure 8: Schematic dip section of the Niger-Delta. Modified from Doust and Omatsola (1990) and Stakicher (1995).

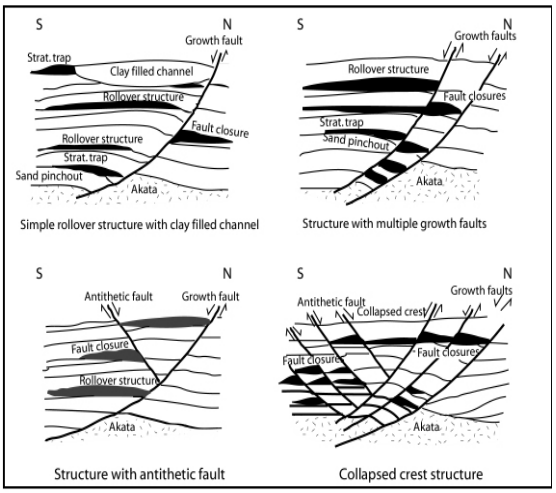

Figure 10: Examples of Niger-Delta oil field structures and associated trap types. Modified from Doust and Omatsola (1990) and Staicher (1995).

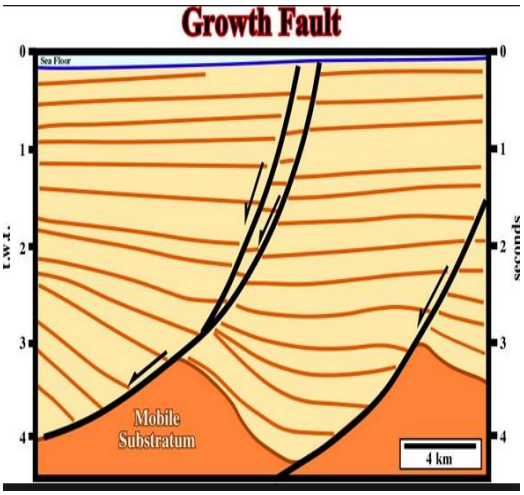

Figure 9: Typical growth faults
Source: Fernando Pessoa University. (2024).

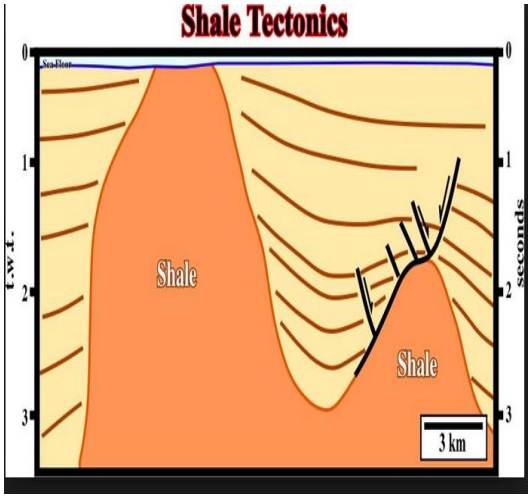

Figure 11: Shale tectonics
Source: Fernando Pessoa University. (2024).

Location/Geology of study area

The study field is located within the Niger-Delta province which is located within Gulf of Guinea (figure 12).

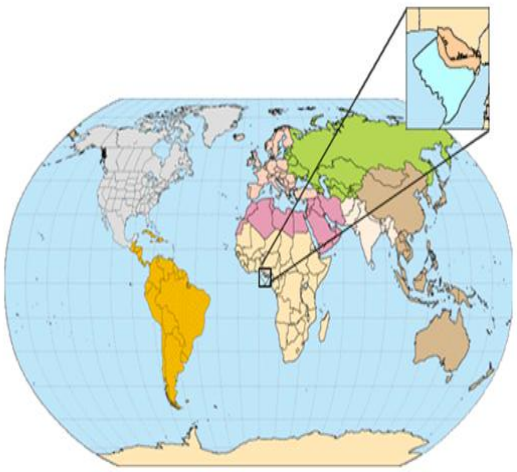

Figure 12: Locaation of Niger-Dela Basin (Gulf of Guninea, Afriica).
Sourice: Tuittle et.al., (1999)

The delta was created in a rift triple junction associated with the development of the Southern part of the Atlantic and which began during the Late Jurassic –Cretaceous. In the Eocene to the Present the delta has pro graded southward as a result of Avulsion and deposition of Depobelts (Doust and Omatsola, 1990). These depobelts constitute the largest regressive deltas globally by area with approximately 300,000 km2 of space (Kulke, 1995), or volume of approximately 500,000 km3 (Hospers, 1965) and thickness over 12 km at the depo-center of the basin. The Niger-Delta geology is biased on that of southern Nigeria and southern Cameron (figure 13). Its northern boundary is the Benin Flank which is a hinge line that trends east-northeast south of the West Africa basement massif. The Cretaceous outcrops on the Abakaliki High form its northeastern boundary. Its southern boundary is the Calabar Flank a hinge line that abuts the nearby Precambrian. The Cameroon volcanic line to the east forms its offshore boundary. The Dahommy Basin the easternmost West African transform-fault passive margin forms its western boundary.

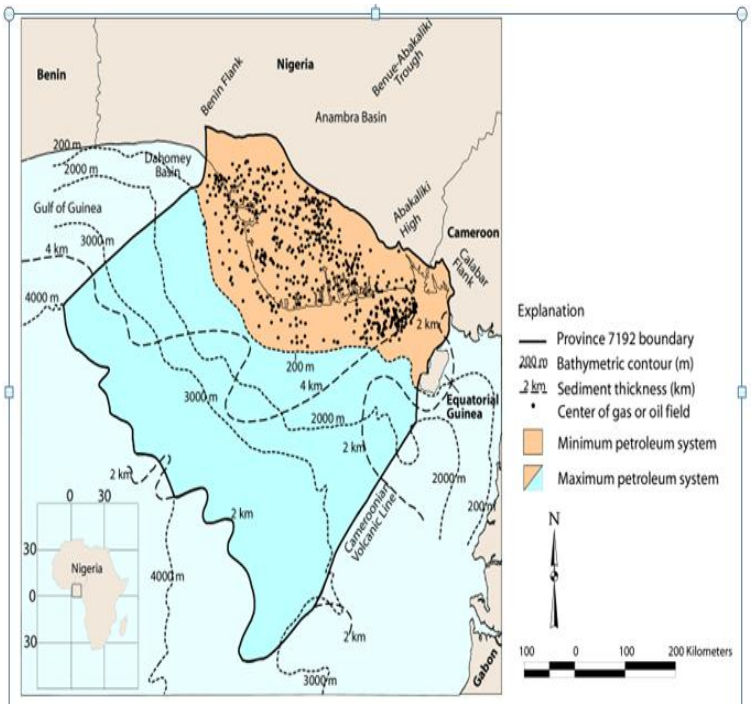

Figure 13: Niger-Delta map indicating (petroleum system):
Source: Petro consultants, (1996)

III. METHODOLOGY (MATERIALS AND METHODS)

Data acquisition

The wireline log data) for an exploratory well code named LAR 015 for trade secret reasons acquired from the Masa Field in one of the sedimentary basins in Nigeria was used for this study. Quality assurance and check were carried out on the data before been loaded into the Schlumberger Petrel 2014 software for further analysis. Gamma ray and resistivity logs were used for the identification of lithology, reservoir and seal in the wellbore. Mechanical properties of rocks (elastic and inelastic properties) were determined using sonic compressional ($\blacktriangle T_C$), shear ($\blacktriangle T_S$) transit tines and density. The estimated elastic properties were Young's modulus (E), Poison's ratio (V), Bulk and Matrix/Grain moduli (K_b and K_m), Shear/Rigidity moduli (G), Bulk compressibility (C_b), Grain compressibility (C_r), and Biot's coefficient (α). Also the inelastic properties were fracture gradient rock strength (uniaxial compressive strength (UCS), tensile (T_o), and cohesive (C_o) strengths.

Nature/Source of Data

Well log data from an exploratory well from the Masa Field comprising of sonic, density, neutron compressional ($\blacktriangle T_C$) and shear ($\blacktriangle T_S$) transit times were used to determined mechanical properties of rocks. Poison's ratio and Young's modulus were gotten using Primary and Secondary wave velocity.

Materials

The material used in this research work include:

- Well log data of a well (LAR 015) from Masa Field (Figure 14).

- Schlumberger Petrel 2014 software used for data analysis
- Laptop used as a work-station
- Ms excel [visual basic.net]

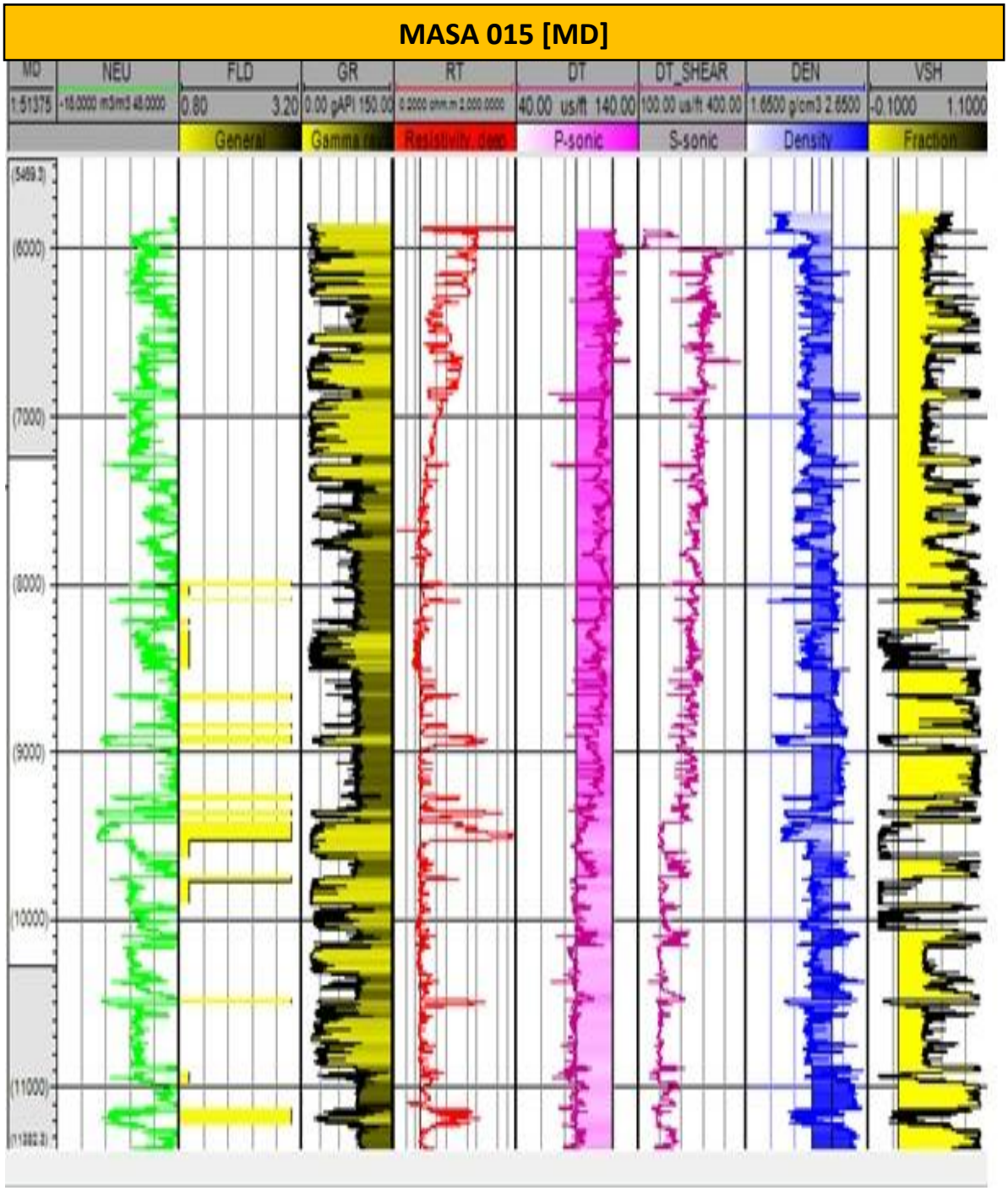

Figure 14: Well 015 in showing well log data

Method of Data collection

The following rock mechanical properties:

Young's modulus (E), Poison's ratio ($_V$), Shear modulus (G), Bulk modus (K_b), Matrix/Grain modulus (K_m), Bulk and Gran compressibility (C_b and C_r) and Biot's coefficient (α) were gotten from the wireline logs using empirical relationships as shown in the equations below:

$V_P = 30.4878/\blacktriangle T_C$ (1)

$V_S = 30.4878/\blacktriangle T_S$ (2)

$V_S = (0.804 \times V_P) - 0.856$ (3)

- **Poison's ratio (v)** = $0.50(Vp/Vs)^2 - 1/(Vp/Vs)^2 - 1$ (4)
  Poisson's ratio (v) was determined using compressional wave ($\blacktriangle T_c$) and shear wave ($\blacktriangle T_s$) ratio as in equation 4
- **Shear Modulus (G):**
  This is the ratio of shear stress to shear strain, it was determined using equation 5
  $G = a\rho/\blacktriangle T_s v$ (5)
  Where coefficient a =0 1.3464, ρ_b = bulk density, $\blacktriangle T_s$ = shear sonic transit time.

- **Young's Modulus (E)**
  $E = x\ 2G(1+v)$ (6)
  Yong's modulus was determined from shear modulus and poison's ratio as in equation 6
- **Bulk Modulus (K_b)**
  This was determined using sonic and density as shown in equation 7
  $K_b = a\rho_b(1/\blacktriangle T_c^2 - 4/3\blacktriangle T_s^2)$ (7)
- **Matrix/Grain Modulus K_m**
  This was determined using equation 8
  $K_m = KS\rho_{ma}/(1/\blacktriangle T_{cma}^2 - 4/3\blacktriangle T_{sma}^2)$ (8)
- **Bulk Compressibility (C_b)**
  This was determined using equation 9 as shown below
  $C_b = 1/K_b$ (9)
- **Rock Compressibility (C_r)**
  This was determined from equation 10 as
  $C_r\ 1/(a\rho_{log}(1/\blacktriangle T_{cma}^2 - 4/3\blacktriangle T_{sma}^2)$ (10)

- **Biot's Coefficient (α)**
  This was determined using equations 11 and 12
  $\alpha = 1 - K_b/K_m$. (11)
  xK_b and xK_m are bulk and matrix modulus respectively
  $\alpha = 1 - C_{rx}/C$ (12)
  C_r and C_b represent matrix and bulk compressibility.
- **Unconfined Compressive Strength (UCS)**
  This was determined using the relationship in equations 13 and 14
  $xUCSx\ 1200\ exp^{(-0.036\blacktriangle T_c)}$ for Sandstones (13)
  $USC = 10(304.8/\blacktriangle T_c - 1)$ for Shale. (14)
- **Shear Strength** Tensile strength (T_o) and initial shear strength (Ƭ) were determined using the empirical relationships in equations 15 and 16
  $T_o = C_o/12$. (15)
  Where C_o = cohesive strength = $5(V_p - 1)/0.5(V_p)$
  $Ƭ_i = 0.026E/C_b \times 10^6(0.008V_{sh} + 0.0045(1 - V_{sh})$. (16)
  Where E = Elastic modulus, C_b = bulk compressibility and V_{sh} = volume of shale.

- **Magnitude and Orientation of In-sit Stress Determination**
  - **I. Vertical stress ($б_v$)**
    This was determined by integrating density (ρ_b) of the materials from the surface to the depth of interst as in equation 17
    $б_v = ∫^2\rho_b(z)gdz$ (17)
    $б_v$ vertical stress, ρ_b = bulk density, z = depth, g = acceleration due to gravity.
  - **II. $б_h$ Minimum Horizontal Stress**
    This was determined using equation 18
    $б_h = v/1\text{-}v(б_v - \alpha P_o) + \alpha P_o$ (18)
    v = poison's ration, α = Bot's coefficient and P_o = Pore Pressure.
  - **III. Maximum Horizontal Stress**
    This was determined using equations 19 and 20 as
    $б_H = б_h + tf\ X\ (Sv - б_h)$ (19)
    $б_H - P_p = 3(б_h - P_p)$ (20)
    where tʃ = tectonic factor, $б_H$ = Maximum horizontal stress, $б_h$ = Minimum horizontal stress and P_p = Pore Pressure.
- **Determination of Fracture Gradient P_{fp}**
  This was determined from empirical relationships using equation 21

$P_{fp} = 3v/2(1 - v)(б_v - P_p) + \alpha P_p$ (21)

P_{fp} = fracture pressure gradient, $б_v$ = vertical stress, α = Biot's coefficient, P_p = pore pressure gradient.

- **Ben Eaton Correlation (F)**
  This was determined using equation 22
  $F = x\ (S\text{-}P/D)\ X\ (v/1\text{-}v) + P/Dx$. (22)
  Where S = overburden stress/vertical stress (psi) and v = poison's ratio
- **Matrix Stress ($б_{ma}$)**
  This was computed using equation 23
  $S = P + б_{ma}$. (23)
  S = overburden stress (psi), P = pore pressure (psi), and $б_{ma}$ = matrix stress (psi)
- **Hubbert and Willis**
  This was determined using the relationships in equations 24 and 25
  $xF_{min} = 1/3(1 + 2P/D)x$ (24)
  $F_{max} = 1/2(1 + 2P/D)$. (25)
  F = fracture gradient, P = pore pressure and D = depth
- **Mathews and Kelly**
  This was computed using equations 26 and 27
  $F = P/D + K_i б_{ma}/D$. (26)
  $F = 1/D(б_{min} + P_f)$ (27)

Method of Data Analysis (Geo-mechanical Model Approach)

There are six components used in building a geo-mechanical model (Figure 15).

Figure 15: Geo-mechanical model
Source: Bowling, (2012).

The simplest geo-mechanical model assumes the subsurface stress field is based mainly on rock linear elastic response to the overburden load. When loaded, the block would strain in the X and Y (S_{Hmax} and S_{hmin}) transverse direction according to Hook's Law.

Three perpendicular stresses exist at any point in the ground,

I. The vertical stress ($б_v$)
II. The Maximum Horizontal Stresses ($б_H$)
III. The Minimum Horizontal Stresses ($б_h$)

The vertical stress ($б_v$) also known as overburden stress is due to the weight of the overlying formations and the fluids they contain. The overburden stress normally tends to spread and this expands the underlying rocks in horizontal lateral directions, as a result of Poison's ratio.

This movement is restricted by the lateral stresses; Maximum and Minimum horizontal stresses.

In this work, Ben Eatons Correlation, Hubbert and Willis, Mathews and Kelly, Bulk, Shear, ad Yong's modulus as well as Poison's ratio empirical methods were used to generate the data used to develop geo-mechanical model.

IV. RESULTS AND DISCUSSION

Presentation of Data

The tables and graphs below show the results obtained in the course of this work.

Table 1. Parameters from logs

S/N WELL	Depth (m)	Rock type	GR log	▲T_c (us/ft)	▲T_s (us/ft)	P_b (g/cm^3)	R (Ωm)	Neu log	V_{sh}
1 LAR 015	6000	Sst.	16.62	120.89	206.37	2.0990	88.8126	27.7116	0.4408
2	6500	Sst./Sh.	67.51	109.25	266.42	2.3340	5.3370	38.0268	0.7643
3	7000	Sst.	22.09	105.95	260.56	2.2250	5.5136	21.9726	0.4672
4	7500	Sh.	87.73	115.01	278.82	2.3398	1.8480	44.6794	0.8544
5	8000	Sst./Sh.	50.04	92.22	207.68	2.4240	5.7410	30.6365	0.7379
6	8500	Sst.	13.47	102.70	240.96	2.1175	0.9535	29.5865	0.0496
7	9000	Sh.	92.71	104.27	239.37	2.4418	1.6315	49.1657	0.2875
8	9500	Sst.	89.84	89.84	158.83	2.0140	1362.1840	5.1850	0.0650
9	10000	Sst.	29.87	93.00	174.09	2.1429	1.2519	30.6153	0.1113
10	10500	Sst.	29.30	91.65	168.67	2.0120	111.5229	9.9630	0.1350
11	11000	Sh.	91.83	97.84	21o.03	2.5050	1.7266	47.5673	1.0000

Sst. = Sandstones, Sh. = Shale, GRlog = Gamma Ray log, ▲T_c = Compressive Sonic transit time, ▲T_s = Shear Sonic transit time, P_b = Bulk density, R = Resistivity, Neu log = Neutron log, V_{sh} = Volume of Shale, NA = Not Available

Table 2: Elastic properties of rocks

S/N WELL	Depth (m)	Rock type	V	G (MPa)	E (MPa)	K_b (MPa)	K_m (MPa)	C_b (MPa)	C_r (MPa)	α
1 LAR 015	6000	Sst.	0.11	1.19 *10^{-9}	2.65 *10^{-8}	160479	2.36 *10^{-9}	6.23 *10^{-6}	6.23 *10^{-6}	1
2	6500	Sst./Sh.	1.81	6.52 *10^{-9}	3.66 *10^{-8}	297404	1.71 *10^{-9}	3.36 *10^{-6}	3.36 *10^{-6}	1
3	7000	Sst.	1.62	7.10 *10^{-9}	3.72 *10^{-9}	271201	9.05 *10^{-9}	3.69 *10^{-6}	3.69 *10^{-6}	1
4	7500	Sh.	1.77	6.38 *10^{-9}	3.54 *10^{-9}	326542	1.04 *10^{-9}	3.07 *10^{-6}	3.07 *10^{-6}	1
5	8000	Sst.Sh.	1.34	1.17 *10^{-9}	5.49 *10^{-9}	187687	1.46 *10^{-6}	5.33 *10^{-6}	5.33 *10^{-6}	1
6	8500	Sst.	1.57	7.52 *10^{-9}	8.62 *10^{-9}	220712	2.32 *10^{-9}	4.53 *10^{-6}	4.53 *10^{-6}	1
7	9000	Sh.	1.44	1.08 *10	9.57 *10^{-9}	251167	3.73 *10^{-9}	3.98 *10^{-6}	3.98 *10^{-6}	1
8	9500	Sst.	0.24	6.99 *10^{-9}	1.46 *10^{-9}	91209	6.25 *10^{-9}	1.09 *10	1.09 *10	1
9	10000	Sst.	0.47	3.55 *0^{-9}	3.79 *10^{-9}	116590	6.79 *10^{-8}	8.58 *10^{-6}	8.58 *10^{-6}	1
10	10500	Sst.	0.39	4.04 *10^{-9}	4.86 *10^{-8}	102758	2.63 *10^{-8}	9.73 *10^{-6}	9.73 *10^{-6}	1
11	11000	Sh.	1.09	1.48 *10^{-9}	2.52 *10^{-9}	198373	7.73 *10^{-8}	5.04 *10^{-6}	5.04 *10^{-6}	1

Sst. = Sandstones, Sh. = Shale, V = Poison's ratio, G = Rigidity/Shear Modulus, E = Young's Modulus, K_b Bulk Modulus, K_m = Matrix Modulus, C_b = Bulk Compressibility, C_r = Rock Compressibility, α = Bot's Coefficient

Table 3: Rock strength profile across the well

S/N Well	Depth (m)	Rock type	UCS (MPa)	C_o (MPa)	T_o (MPa)	ζ_i (MPa)	$V_{sh\ (frac)}$
1 LAR 015	6000	Sst.	25.42	29.65	2.47	9.23 *10^{-9}	0.44
2	6500	Sst./Sh.	28.16	25.83	2.15	3.04 *10^{-9}	0.76
3	7000	Sst.	29.04	24.75	2.06	3.29 *10^{-9}	0.47

4	**7500**	**Sh.**	**26.73**	**27.72**	**2.30**	**$2.29 *10^{-9}$**	**0.85**
5	**8000**	**Sst./Sh.**	**33.41**	**58.12**	**4.84**	**$8.73 *10^{-9}$**	**0.74**
6	**8500**	**Sst.**	**29.97**	**23.68**	**1.97**	**$8.14 *10^{-9}$**	**0.05**
7	**9000**	**Sh.**	**29.51**	**24.19**	**2.02**	**$8.73 *10^{-9}$**	**0.29**
8	**9500**	**Sst.**	**34.31**	**19.46**	**4.43**	**$5.65 *10^{-9}$**	**0.07**
9	**10000**	**Sst.**	**33.13**	**20.51**	**1.71**	**$1.80 *10^{-9}$**	**0.11**
10	**10500**	**Sst.**	**33.62**	**20.06**	**1.67**	**$6.80 *10^{-9}$**	**0.14**
11	**11000**	**Sh.**	**31.47**	**22.09**	**1.84**	**$1.25 *10^{-9}$**	**1.00**

UCS = Unconfined Compressive strength, C_o = Cohesion, T_o = Tensile strength, τ_i = Initial Shear stress, V_{sh} =Volume of Shale

Table 4: Typical In-situ and wellbore stress profile

S/N Well	Depth (m)	Rock type	$б_v$ (MPa/Km)	$б_H$ (MPa/Km)	$б_h$ (MPa/Km)
1 LAR 015	**6000**	**Sst.**	**37.78**	**55.07**	**24.33**
2	**6500**	**Sst./Sh.**	**49.31**	**23.08**	**12.46**
3	**7000**	**Sst.**	**54.51**	**42.78**	**14.26**
4	**7500**	**Sh.**	**65.81**	**47.69**	**39.15**
5	**8000**	**Sst./Sh.**	**77.57**	**44.10**	**12.20**
6	**8500**	**Sst.**	**76.49**	**77.05**	**66.91**
7	**9000**	**Sh.**	**98.89**	**83.18**	**17.47**
8	**9500**	**Sst.**	**90.88**	**87.03**	**44.33**
9	**10000**	**Sst.**	**10.71**	**47.55**	**15.15**
10	**10500**	**Sst.**	**11.09**	**98.16**	**16.65**
11	**11000**	**Sh.**	**13.78**	**52.70**	**52.70**

$б_v$ = Vertical stress, $б_H$ = Maximum Horizontal stress, $б_h$ = Minimum Horizontal stress

Table 5: Formation pressure and fracture pressure gradient profile

S/N Well	Depth (ft)	Rock type	P_f (psi	F_{pg} (psi/ft) Eaton's correlation	F_{pf} (Psi/ft) Mathew and Kelly	F_{pf} (Psi/ft) Hubbert and Willis (Min)	F_{pf} (Psi/ft) Hubbert and Willis (Max)
1 LAR 015	**6000**	**Sst.**	**2790**	**0.4055**	**0.4587**	**0.6433**	**0.965**
2	**6500**	**Sst./Sh.**	**3023**	**0.4809**	**0.4727**	**0.6434**	**0.9651**
3	**7000**	**Sst.**	**3255**	**0.4568**	**0.4681**	**0.6433**	**0.965**
4	**7500**	**Sh.**	**3488**	**0.4651**	**0.4738**	**0.6434**	**0.9651**
5	**8000**	**Sst./Sh.**	**3720**	**04451**	**0.47**	**0.6433**	**0.965**
6	**8500**	**Sst.**	**3953**	**0.7872**	**0.4694**	**0.6434**	**0.9651**
7	**9000**	**Sh.**	**4185**	**1.5002**	**0.4695**	**0.6433**	**0.965**
8	**9500**	**Sst.**	**4418**	**0.4667**	**0.4696**	**0.6434**	**0.9651**
9	**10000**	**Sst.**	**4650**	**1.0563**	**0.8229**	**0.6433**	**0.965**
10	**10500**	**Sst.**	**4888**	**0.7716**	**0.4604**	**0.6434**	**0.9650**
11	**11000**	**Sh.**	**5115**	**0.5083**	**0.4616**	**0.6433**	**0.965**

P_f = Formation pressure, F_{pg} = Formation pressure gradient

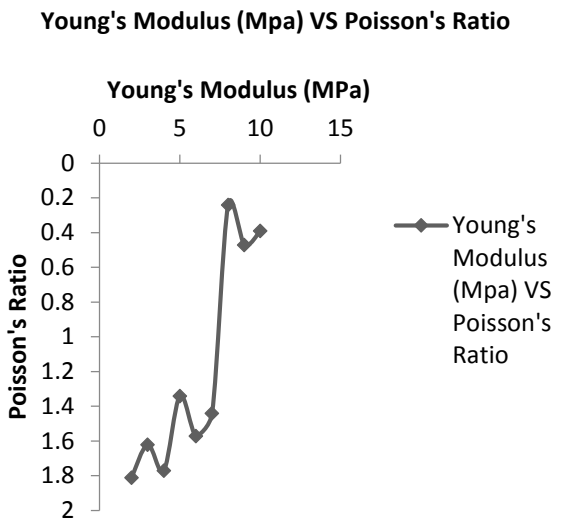

Figure 16: Young's modulus (MPa) vs Poisson ratio plot showing sandstone brittleness and shale ductility

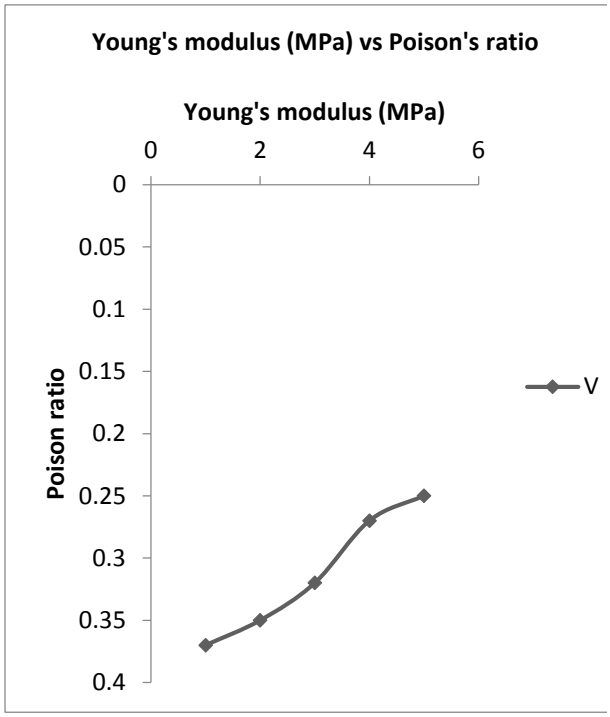

Figure 17: Young's modulus (MPa) vs Poisson ratio plot showing sandstone brittleness and shale ductility

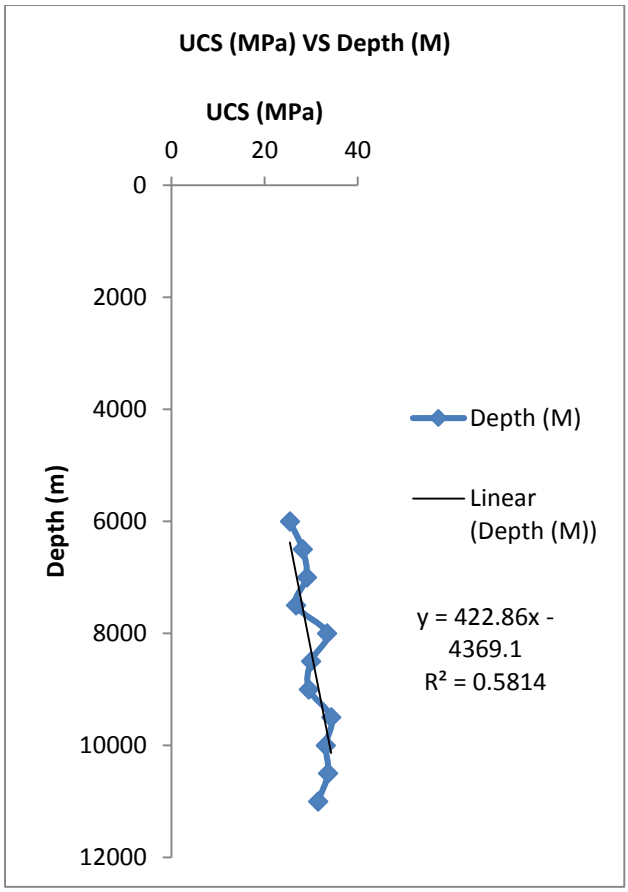

Figure 18: Uniaxial compressive strength (UCS) (MPa) VS depth (m) plot

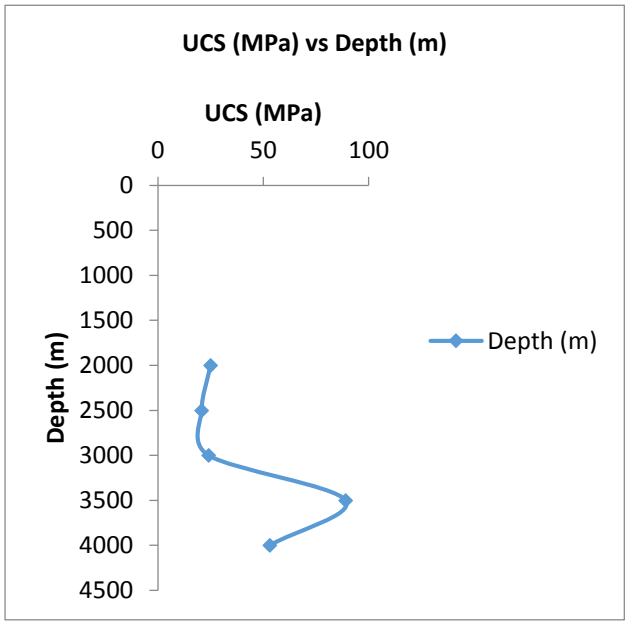

Figure 19: Uniaxial compressive strength (UCS) (MPa) VS depth (m) plot

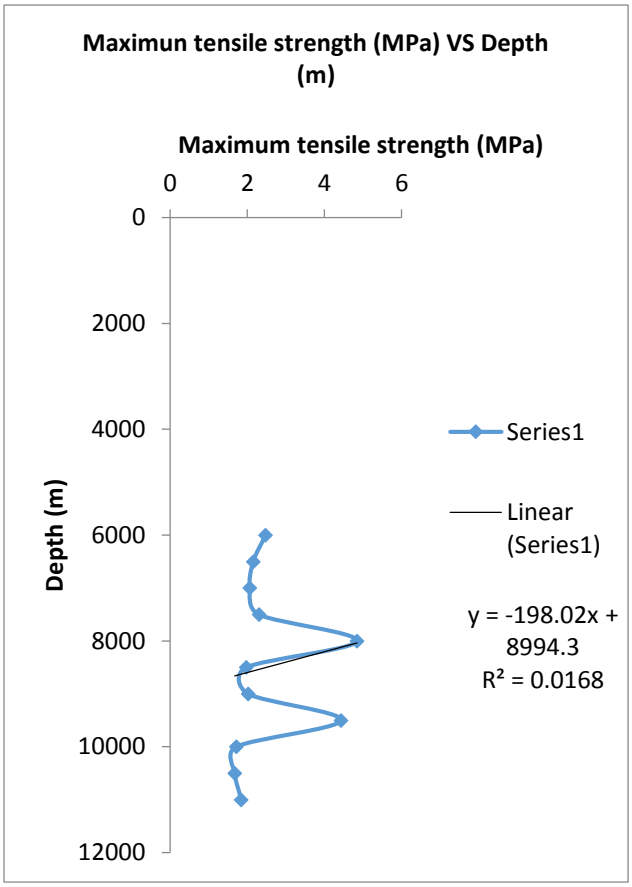

Figure 20: Maximum tensile strength (MPa) vs depth (m) plot

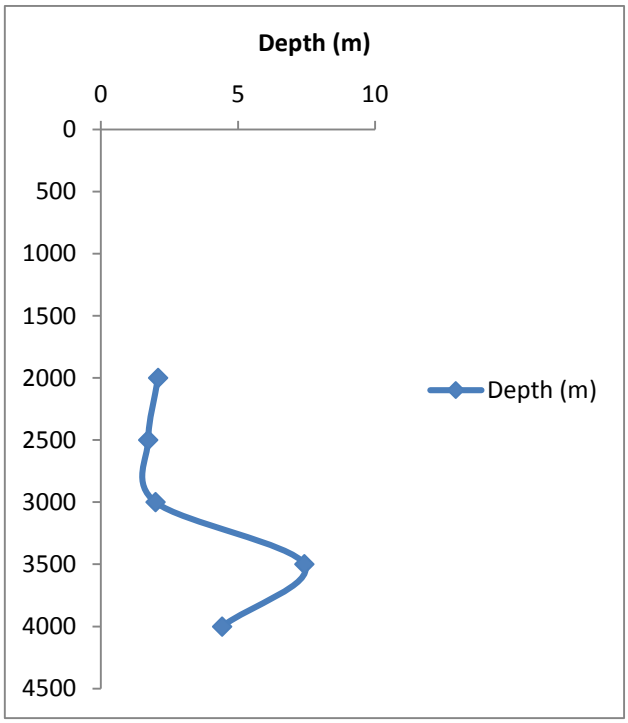

Figure 21: Maximum tensile strength (MPa) vs depth (m) plot

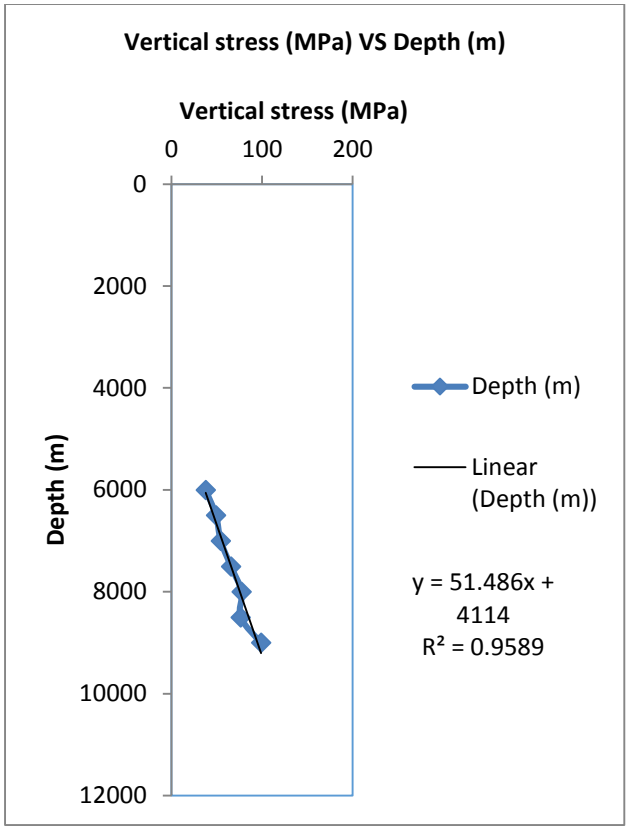

Figure 22: Vertical stress (MPa) vs depth (m) plot

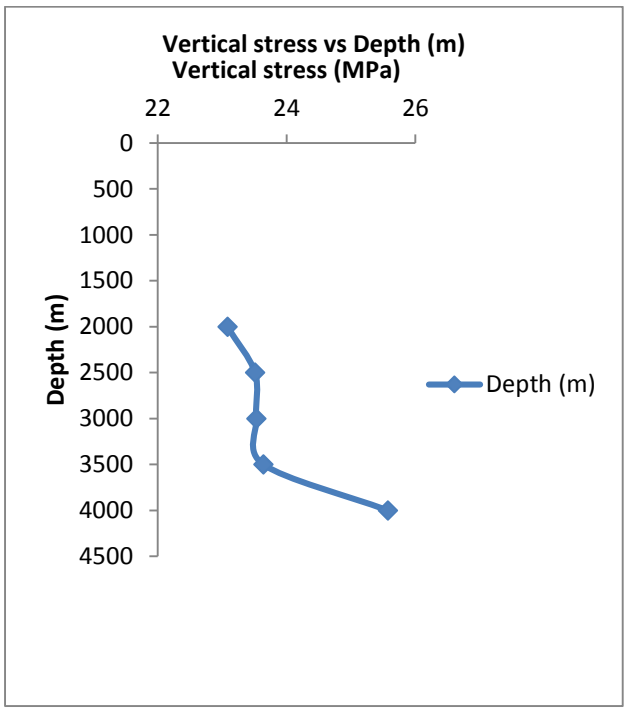

Figure 23: Vertical stress (MPa) vs depth (m) plot

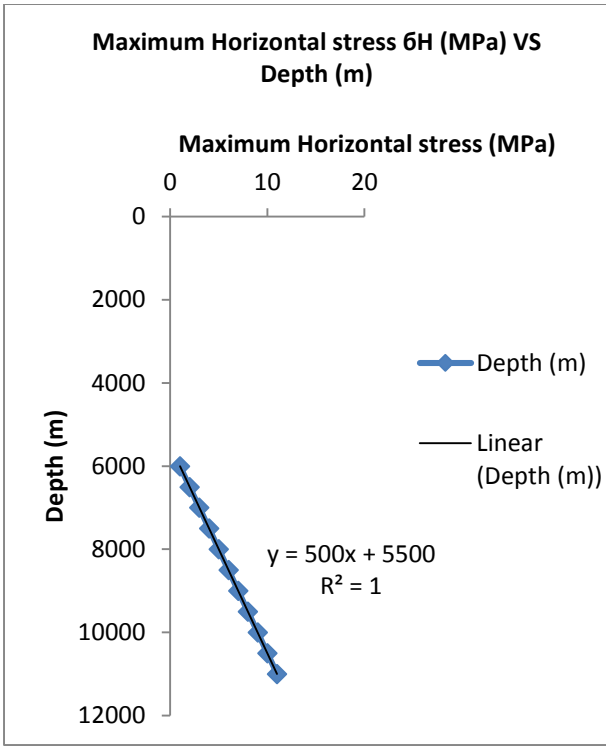

Figure 24: Maximum horizontal stress (MPa) vs depth (m) plot

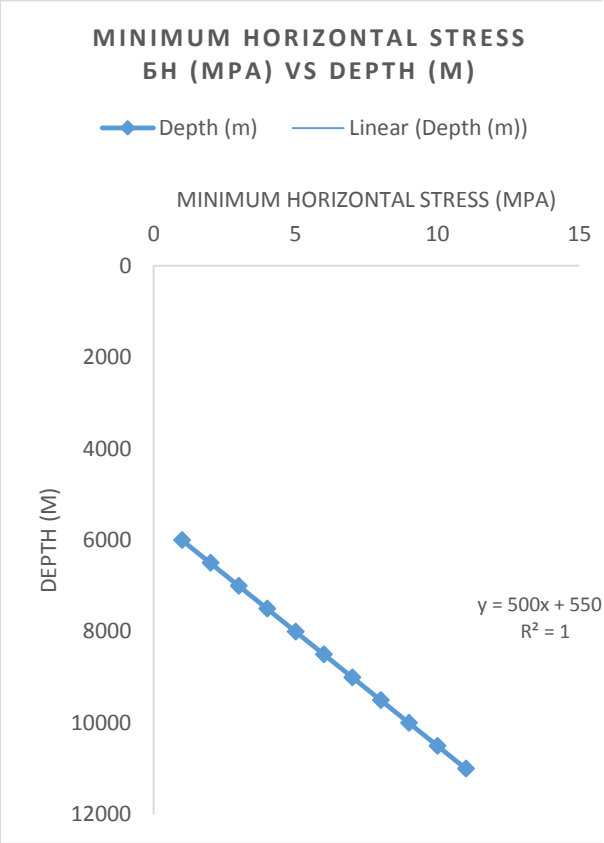

Figure 25: Minimum horizontal stress (MPa) vs depth (m) plot

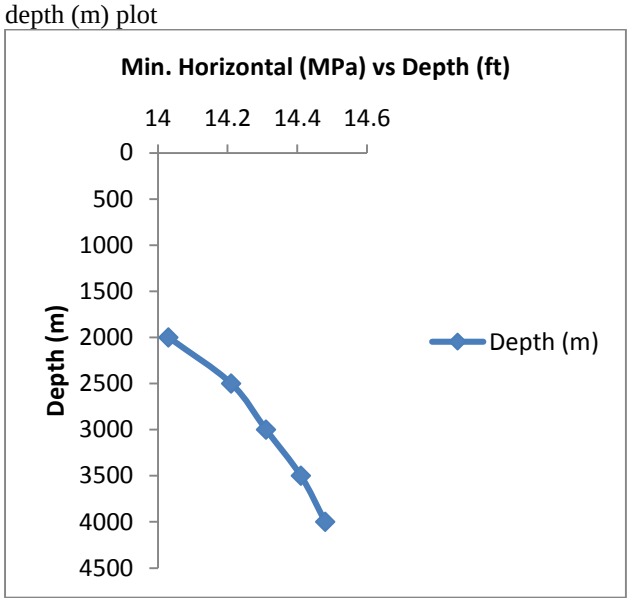

Figure 26: Minimum horizontal stress (MPa) vs depth (m) plot

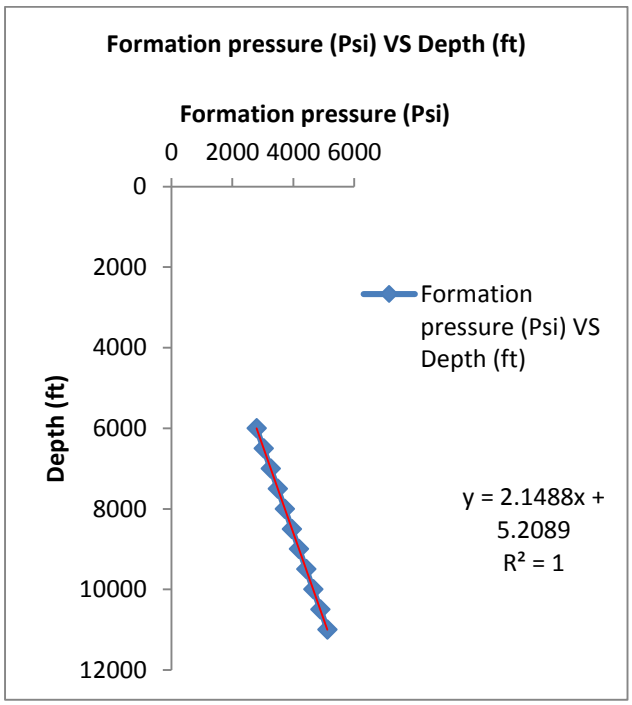

Figure 27: Formation pressure (psi) vs depth (ft) plot

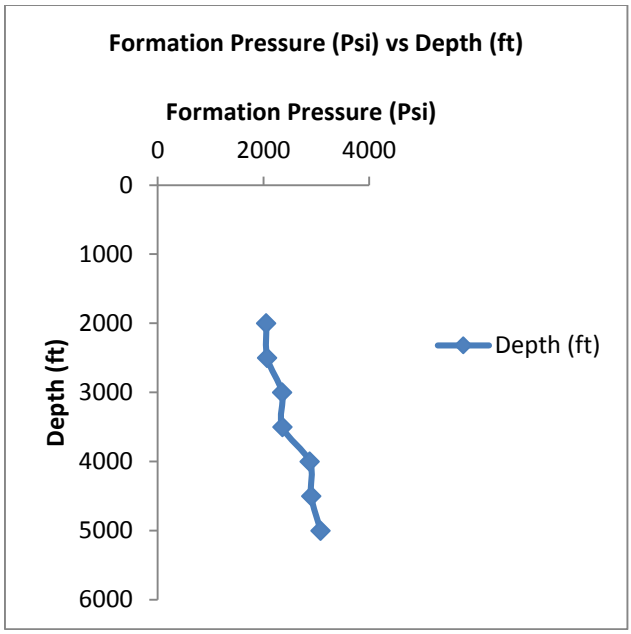

Figure 28: Formation pressure (psi) vs depth (ft) plot

V. Data Analysis

The depth of investigation range from 6000m to 11000m in the subsurface with stratigraphic succession made up of intercalations of Shale and Sandstones. Rock mechanical property estimates are given using log parameters. A summary of the rock strength and elastic properties that were obtained from empirical correlations is provided (table 1 -5). Shale has high bulk rigidity elastic and average Poisson ration moduli of 1. 80 9. 57*10-9 (MPa) 326542 (MPa) and 6. 38*109 (MPa) respectively. But shale is more ductile stiffer less compressive and more likely to experience compressive shear failure because of its low bulk compressibility and rock strength. Sandstones are more brittle and more likely to experience tensile failure because they have higher compressibility and rock strength but comparatively lower Poison ratio elastic bulk and rigidity moduli. Weak shale and shale within sandstones can experience wellbore failures due to low rock strength. The bulk and matrix moduli and the rigidity modulus of the rock seem to be generally declining while the formation pressure and elastic modulus of the rock appear to be increasing with depth (fig. 27 – 28). A summary is provided of the assessed in-situ wellbore stress magnitudes. The magnitudes of the stress gradients (vertical) vary throughout the field from 37. 78 MPa/Km at 6km to 98. 89 MPa/Km at 9km. Because overburden loading increases with burial depth vertical stress increases as well. The vertical stress trend was assumed by the magnitudes of the maximum and minimum horizontal stresses. In addition the horizontal stress ranges from 24 to 33 MPa/Km at 6 km to 52 to 69 MPa/Km at 11 km true vertical depths and from 55 to 80 MPa/Km at 11 km.

VI. Discussions

The data analysis reveals significant insights into the mechanical properties and stress conditions of the subsurface formations investigated, ranging from 6000m to 11000m in depth. Different mechanical behaviors that affect wellbore stability are presented by the stratigraphic succession which is defined by sandstone and shale intercalations. The ductility and stiffness of shale formations are indicated by their high bulk modulus elastic modulus rigidity modulus and average Poissons ratio. They are more vulnerable to compressive shear failure though because of their low bulk compressibility and rock strength. This brittleness contrasts with the ductility and stiffness of sandstones which have higher compressibility and rock strength but lower Poissons ratio elastic modulus bulk modulus and rigidity modulus. Sandstones are more likely to experience tensile failure due to their brittleness.

The observed wellbore failures in shale and weak shale within sandstones can be attributed to the low rock strength of these formations. The intricate relationship between mechanical characteristics and stress conditions is highlighted by the general trend of decreasing rigidity bulk and matrix moduli with depth along with an increase in formation pressure and elastic modulus. Significant variation across the field is indicated by the in-situ wellbore stress magnitudes. The vertical stress gradients are 37-78 MPa/km at 6km and 98-89 MPa/km at 9km which illustrate how overburden loading causes vertical stress to increase with depth. Maximum and minimum horizontal stresses range from 55. 07 MPa/km at 6km to 55. 80 MPa/km at 11km while minimum

horizontal stresses range from 24. 33 MPa/km at 6km to 52. 69 MPa/km at 11km to mirror the trend of vertical stress (fig. 16 – 28).

These findings underscore the importance of understanding the mechanical properties and stress conditions of subsurface formations for effective wellbore stability management. The variations in stress magnitudes and mechanical properties with depth necessitate tailored strategies for drilling and wellbore stability to mitigate the risks of wellbore failure. The data derived from well logs and empirical correlations provide a robust foundation for developing such strategies, ensuring safer and more efficient drilling operations.

VII. CONCLUSIONS

The investigation into the mechanical properties and stress conditions of subsurface formations from 6000m to 11000m depth has provided valuable insights into wellbore stability. The distinct behaviors of shale and sandstone formations, characterized by their respective ductility and brittleness, significantly influence wellbore integrity. Shale's susceptibility to compressive shear failure and sandstone's potential for tensile failure highlight the need for tailored drilling strategies. The observed trends in mechanical properties and stress magnitudes with depth underscore the complexity of subsurface conditions. The increase in vertical stress with depth due to overburden loading and the corresponding trends in horizontal stresses necessitate a comprehensive understanding of these factors for effective wellbore stability management. The data derived from well logs and empirical correlations form a robust foundation for developing strategies to mitigate wellbore instability. By leveraging these insights, drilling operations can be optimized to reduce non-productive time and enhance overall safety and efficiency. This research contributes to the broader field of petroleum engineering by providing practical solutions for managing wellbore stability in complex geological settings.

REFERENCES

[1]. Agushoe. (2011). The hole problem: Sloughing shale. Retrieved December 4, 2024, from https://agushoe.wordpress.com/2011/06/08/the-hole-problem-sloughing-shale/
[2]. Azizi, V. and H. Memarian, 2006. S wave velocity estimation for evaluating geomechanical properties of rocks in oil and gas wells of Iran. Proceedings of the 1st Iranian Petroleum Engineering Congress, May30-31, Tehran.
[3]. Bowling, D. (2012). Introduction to BHI's Geomechanical Capabilities in the Asia Pacific Region: Rules of Thumb, Information on Future Technology. Baker Hughes Inc.
[4]. Drilling Formulas. (2024.). Drilling Formulas. Retrieved December 4, 2024, from https://www.drillingformulas.com/
[5]. Fernando Pessoa University. (2024). Basic principles in tectonics: Fault displacements. Retrieved December 4, 2024, from http://homepage.ufp.pt/biblioteca/WebBasPrinTectonics/BasPrincTectonics/Page9.htm#FaultDisplacements
[6]. Mechanics Mining Science,, 957-973.
[7]. Onikoyi, A.S., Nwabueze, V.O., Okoro, F.O., and Ajienka, J.A., (2014). 'Review of Sand Production from Oil Well Completions Across Depositional Environments in the Niger Delta', SPE Conference paper 2014, Paper ID: SPE-172484-MS, pp. 12
[8]. Petroconsultants, 1996, Petroleum exploration and production database: Houston, Texas, Petroconsultants, Inc., [database available from Petroconsultants, Inc., P.O. Box 740619, Houston, TX 77274-0619].
[9]. Short, K. C. and Stauble, A. J. (1967).Outline of Geology of the Niger Delta. American Association of Geologists, Vol. 51, No. 5, pp. 761-779.
[10]. Stacher, P. (1995) Present Understanding of the Niger Delta Hydrocarbon Habitat. In: Oti, M.N. and Postma, G., Eds., Geology of Deltas, A.A. Balkema, Rotterdam, 257-267.
[11]. Tan, N. (2013). Well design. New Mexico Technology Science University, 413.
[12]. Tuttle, M. L. W., Charpentier, R. R., & Brownfield, M. E. (1999). The Niger Delta Petroleum System: Niger Delta Province, Nigeria, Cameroon, and Equatorial Guinea, Africa (Open-File Report 99-50-H). U.S. Geological Survey. Retrieved December 4, 2024, from https://pubs.usgs.gov/of/1999/ofr-99-0050/OF99-50H/OF99-50H.pdf